Nonlinear Control Based on Fuzzy Logic for a Wind Energy Conversion System Connected to the Grid

L. BENAAOUINATE*‡, M. KHAFALLAH*, D. VOYER**, A. MESBAHI*, T. Bouragba***

*Laboratory of Energy & Electrical Systems (LESE), Superior National School of Electricity and Mechanical (ENSEM), Hassan II University of Casablanca-20470, Casablanca- Morocco

**Industrial systems engineering school (EIGSI), La Rochelle, France

***Industrial systems engineering school (EIGSI), Casablanca- Morocco

(l.benaaouinate@ieee.org, m.khafallah@gmail.com, voyer@eigsi.fr, abdelouahed.mesbahi@gmail.com, tarik.bouragba@eigsica.ma)

‡ Corresponding Author; L. BENAAOUINATE, 24000, Tel: +212610844961,

l.benaaouinate@ieee.org

Received: 08.01.2020 Accepted:19.02.2020

Abstract- This paper presents, analysis, and simulation of a variable-speed wind turbine control. Wind turbine emulator (WTE) based on induction motor (IM) is used to provide a controlled environment for testing the wind energy conversion system (WECS) control. The permanent magnet synchronous generator (PMSG) is driven by the WTE, and it is tied to the grid via back-to-back converters. The aim of the study is threefold: the development of the WTE, extracting the maximum power, and feeding captured power to the grid. However, the methods of maximum power point tracking (MPPT) using Fuzzy logic is used to maximize the wind power captured at different wind speeds. The grid-tied inverter controlled by the fuzzy adaptative PI controller is used for transferring energy to the grid and maintaining DC-Link voltage constant. Simulation results performed on the Matlab/Simulink environment verify the performance of the proposed control strategies applied on WECS tied to the grid. The used approach overcomes the non-linearity constraint of the DC-Link voltage by using a fuzzy adaptative PI controller instead of the classical PI controller. It also provides an optimal energy gain from the MPPT block based on fuzzy logic.

Keywords Wind turbine emulator (WTE), Field oriented control (FOC), Maximum power point tracking (MPPT), Voltage oriented control (VOC), Fuzzy Logic.

1. Introduction

Factors such as worrying world climate changes resulting from pollution problems, advanced power control, and economic benefits are given considerable attention to wind power as energy sources [1]. Wind Energy Conversion System (WECS) can be categorized into a fixed-speed type and a variable-speed type. As the naming indicates, fixed-speed generators rotate at practically a constant speed and directly connected to the electrical grid. Thus, the turbulence of the wind engenders strongly fluctuating power in the

WECS. Robust mechanical design is required to absorb the high mechanical stresses of this type of turbine [2,3].

However, for variable-speed WECS, the generator adjusts its rotational speed continuously according to the wind speed thanks to the power converters interface provided in its configuration. Thus, variable-speed WECS put forward several benefits, such as the operation at optimal speed using maximum power point tracking MPPT algorithm, the transfer of captured power to the grid, maximum power achieved at different wind speeds, and better efficiency. Therefore, this configuration is turning into the most commercial and the more growth application of wind energy technology [4-7].

In regards to the generators exploited in WECS, PMSG, and doubly-fed induction generator (DFIG) are the most generators used in (WECS) [8,9]. PMSG is becoming more and more commonly used thanks to its robustness, the advantage of no requirement of the gearbox by dint of the very high torque reached at low wind speeds, no notable losses are produced in the rotor system, and no need to the external excitation current. Thus, the performance of the WECS consist of PMSG has been evaluated greater than other configurations, especially for variable-speed wind turbines connected to the electrical grid [10,11].

The back-to-back converters are provided between the generator PMSG terminal and the grid control the PMSG for maximizing the captured power at different wind speed at the generator side. They control and deliver the active and reactive power into the grid by keeping the DC-Link voltage constant at the inverter input.

In the literature, several schemes have been proposed to control the various elements of the wind energy conversion system [12-14]. They consist of back-to-back converters controlled by vector control based on the conventional proportional-integral (PI) controller. These approaches present a limitation i.e., the conventional PI controller could not perform accurately with the nonlinearity of some subsystems in the WECS, especially the DC-link voltage system

A nonlinear approach based on fuzzy logic control is applied to develop an MPPT algorithm without using characteristic data provided by the manufacturer for a given wind turbine to maximize the energy extracted from the wind generator, and to control the grid-tied inverter for DC-Link voltage regulation substituting the proportional-Integral (PI) controller to keep the DC-Link voltage constant.

This paper is structured as listed below: The design of the wind turbine emulator (WTE) based on an induction motor (IM) controlled by field-oriented control (FOC) to reproduce the dynamic behavior of a real wind turbine is detailed in section 2; The development of extracting the maximum power point MPPT algorithm based on fuzzy logic is presented in section 3; The control of PMSG and the control of the grid-tied inverter using voltage-oriented control (VOC) are provided in sections 4 and 5 respectively; The simulation results are discussed in Section 6.

2. Wind turbine emulation

Figure 1 depicts the design of the proposed WECS connected to the grid via a full-capacity back-back converters system. The PMSG is driven by a wind turbine emulator WTE based on an induction motor to substitute the real wind turbine and to provide a testing environment for WECS control strategies in a controlled and safe environment.

With the use of the power converter, the PMSG is fully decoupled from the grid and can operate in full speed range. This also enables the system to perform reactive power compensation and smooth the grid connection.

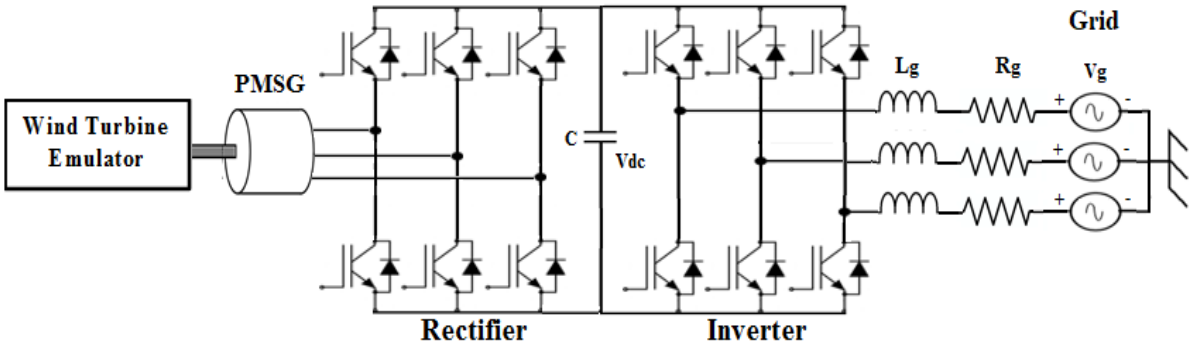

Fig. 1. Wind energy conversion system based on PMSG.

2.1. Wind turbine modelling

The wind turbine cannot wholly capture the wind power available. So, the power extracted may be expressed as [15,16].

$$P_m = \frac{1}{2} C_p(\lambda, \beta) \rho \pi R^2 v^3 \quad (1)$$

Where ρ represents the air density (usually 1.2251 kg/m^3), R represents the radius of the area swept by the wind in (m), C_p represents the power coefficient, and ν represents the wind speed in (m/s) and λ is the tip-speed ratio (TSR).

The power coefficient Cp depends on the TSR λ, which is expressed as:

$$\lambda = \frac{R\, w_m}{v} \tag{2}$$

Where ω_m is the angular speed of the rotor in (rad/s).

The coefficient Cp can be obtained by wind tunnel or simulation. It is in the form of a nonlinear function of λ and β. Heier [17] suggests a more complex expression:

$$C_p(\lambda,\beta) = 0.5109(116.\lambda_i - 0.4.\beta - 5)e^{\frac{-21}{\lambda_i}} + 0.0068.\lambda \tag{3}$$

$$\lambda_i = \frac{1}{\lambda + 0.08\beta} - \frac{0.0035}{\beta^3 + 1} \tag{4}$$

Moreover, the power coefficient is a nonlinear function of the blade pitch angle β (in degrees) and the TSR λ. It achieves the maximum at the particular value of λ called by λ_{opt}. Thus, in order to maximize the captured power by a wind turbine, λ must be maintained at λ_{opt}.

2.2. Wind turbine emulator development

Figure 2 represents the structure of the WTE using an IM controlled by the field-oriented control system. The mathematical model of the wind turbine is developed using equation 1. The torque in the output of the mathematical model depends on the wind velocity with a stochastic profile, and it is then used as a reference in the field-oriented control system. This control system consists of controlling the stator currents of the induction motor by generating pulses to the inverter, and producing a torque depends on the wind velocity similarly required by the electrical generator as the real wind turbine.

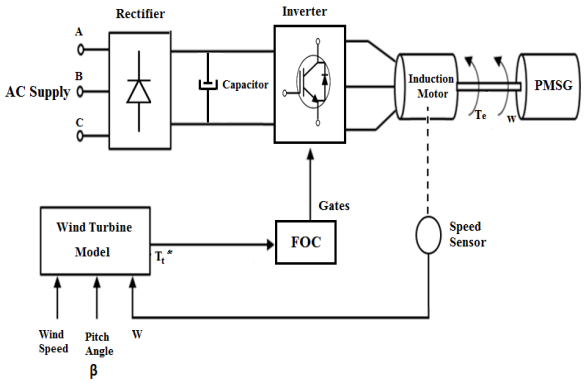

Fig. 2. Structure of the proposed WTE.

The FOC system used to drive the induction motor is based on the identification of the stator currents as two orthogonal components generally related to the rotating magnetic field. One component defines the torque and the other the flux. Which makes the torque of IM proportional to the current and the flux, and it becomes indeed similar to that of DC motor [18].

The torque of the induction motor is defined as:

$$T_e = \frac{3}{2} p \frac{M_{sr}}{L_r} \left(\phi_{rd} I_{sq} - \phi_{rq} I_{sd}\right) \tag{5}$$

With p is pole pairs, M_{sr} and L_r are the mutual inductances, ϕ_{rd} and ϕ_{rq} are the rotor flux in the dq frame, I_{sd} and I_{sq} are the stator currents in the dq frame.

The speed is expressed as:

$$\omega_s = p\Omega + \omega_R \tag{6}$$

The expression of torque as a function of the rotor flux is given equation (5). With the FOC, we impose to orient the rotor flow along with the axis d, in other words, we cancel the component ϕrq. Under these conditions, the torque is reduced to the following expression:

$$T_e = \frac{3}{2} p \frac{M_{sr}}{L_r} \phi_{rd} I_{sq} \tag{7}$$

$$\omega_r = M_{sr} \frac{1}{\tau\, \phi_{rd}} I_{sq} \tag{8}$$

Once the current setpoints have been returned to the abc reference, the hysteresis control technique is implemented. The bang-bang type hysteresis control principle is based on the comparison of sinusoidal reference currents (isa *, isb *, isc *) with the respectively measured phase currents of the machine (isa, isb, isc).

Figure 3 represents the structure of the FOC used to control the IM. In this work, the FOC is applied to drive the IM by a tow-level inverter controlled by hysteresis currents control. Rotor speed Ω and stator currents are measured to define the stator pulsation ωs and the angle of Park θs.

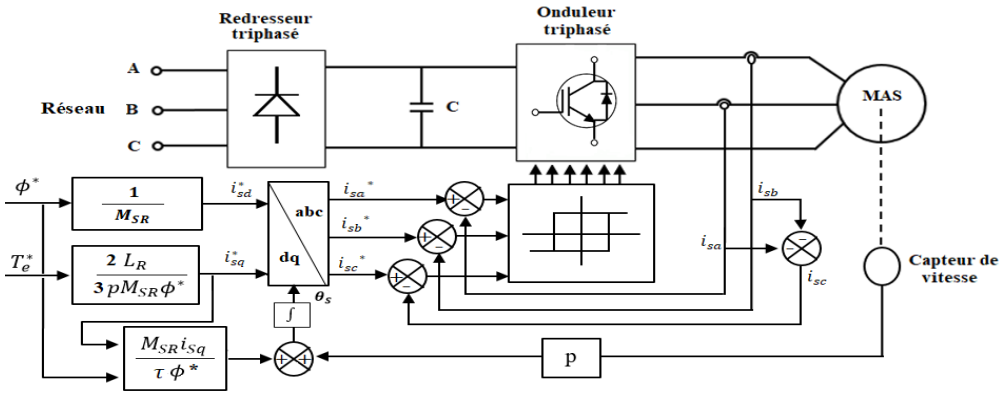

Fig. 3. Structure of FOC used to control the IM.

3. MPPT algorithm based on fuzzy logic

The primary purpose of an MPPT algorithm is to derive the maximum power for specified wind velocity and load by generating a reference speed that corresponds to the optimal power of the wind energy conversion system [19-20].

The structure with a 3-phase PWM rectifier such as figure 1 ensures a dynamic and a reliable control in speed or torque of the PMSG generator, which provides a smooth movement of the operating point over the entire range of rotation and thereby perform research for the desired maximum power without the knowledge of the turbine characteristics curve Cp(λ).

In the absence of any knowledge of the turbine characteristics, rules of behavior to be held to converge towards the optimal point are fairly easy to develop. These rules are based on the variations of power and speed. For example, "if I measure a power increase following a positive speed increment, I must continue to increase the speed." From these language rules, an MPPT based on the fuzzy sets is used.

The MPPT algorithm based on the variation of DC bus power (ΔP) and rotation speed (ΔΩ) generates a reference rotation speed Ω_{ref} according to the following equations:

$$\Delta P = P[k] - P[k-1]$$

$$\Delta\Omega = \Omega[k] - \Omega[k-1] \quad (9)$$

$$\Omega_{ref}[k] = \Omega[k-1] + \Delta\Omega_{ref}[k]$$

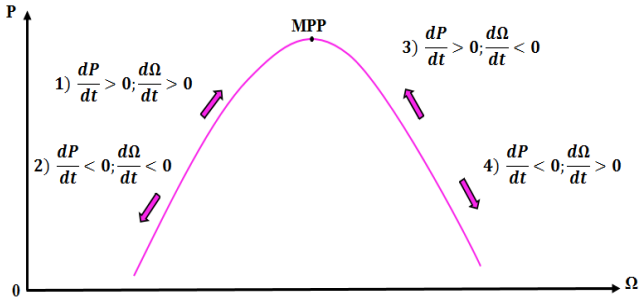

Fig. 4. the four cases for the development of power versus the rotor speed.

Table 1. MPPT output evolution

		$d\Omega/dt$	
		< 0	> 0
$\frac{dP}{dt}$	< 0	2) Bad direction	4) Bad direction
	> 0	3) Good direction	1) Good direction

The major drawback of this method, based on absolute variations of power and speed, is that the variations of speed and power do not have the same weight depending on the operating point of the WECS, i.e., depending on whether the wind velocity is very high or low. The system reacts correctly only in a restricted band of wind speed according to the settings of the MPPT algorithm. Outside this area, it is difficult to adjust the dynamics of the system properly. For this reason, the input/output variables are defined as relative values. These variations are treated with the averages of the quantities measured. Equations (10), (11), and (12) describe this technique.

$$\Delta P = 2.\frac{P[k] - P[k-1]}{P[k] + P[k-1]} \quad (10)$$

$$\Delta\Omega = 2.\frac{\Omega[k]-\Omega[k-1]}{\Omega[k]+\Omega[k-1]} \quad (11)$$

$$\Omega_{ref}[k] = \Omega[k-1]\frac{2+\Delta\Omega_{ref}[k]}{2-\Delta\Omega_{ref}[k]} \quad (12)$$

The theory of fuzzy sets is based on the concept of partial membership. Each element belongs progressively to the membership functions (fuzzy sets) a priori identified. Several membership functions can be defined on the same variable: in the case of figure 4, the variable ΔP always belongs to two membership functions.

Figure 5 presents the block diagram of a fuzzy logic stages. The Fuzzification is the first stage of the fuzzy logic process; it converts the input data into the fuzzy representation using membership functions. The inference is the second stage of the process; it evaluates the rules and generates results using output membership functions. The De-Fuzzification is the third and last stage of the process; it translates the membership functions to a numerical value for Ωref [k].

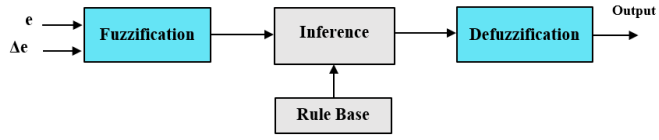

Fig. 5. block diagram of a fuzzy logic stages.

The Fuzzification operation provides a transformation from the real domain to the fuzzy domain. It determines the degree of membership (μ) of an input variable for a given membership function. The degree of membership represents the degree of truth of the membership function.

Table 2. Rules Base for Fuzzy Logic

ΔΩ \ ΔP	HN	AN	lN	Z	lP	AP	HP
HN	HP	HP	AP	Z	AN	HN	HN
AN	HP	AP	lP	Z	lN	AN	HN
lN	MP	lP	lP	Z	lN	lN	AN
Z	HN	AN	lN	Z	lP	AP	HP
lP	AN	lN	lN	Z	lP	SP	AP
AP	HN	AN	lN	Z	lP	AP	HP
HP	HN	HN	AN	Z	AP	HP	HP

The abbreviations used in Table 2 are given by:

HN: Huge Negative; AN: Average Negative; lN: little negative; Z: Zero; HP: Huge Positive; AP: Average Positive: lP: little Positive.

In our case, the center of gravity (COG) approach is used in the De-Fuzzification. This method is based on the sum of the centers of gravity of each sub-area of the total area of the membership function distribution.

The defuzzified value x_0 using COG is expressed as:

$$x_0 = \frac{\sum_{i=1}^{n} x_i \mu_c(x_i)}{\sum_{i=1}^{n} \mu_c(x_i)} \quad (13)$$

With x_i is the sample element $\mu(x_i)$ is the membership function, and n represents the number of the sample element.

4. PMSG control system

In the dq synchronous frame, the stator voltages of the PMSG are expressed as [21-22]:

$$\begin{cases} v_{ds} = -R_s i_{sd} - L_d \dfrac{di_{sd}}{dt} + \omega L_q i_{sq} \\ v_{qs} = -R_s i_{sq} - L_q \dfrac{di_{sq}}{dt} + \omega.\varphi_f \end{cases} \quad (14)$$

Where Rs is stator resistance isd, isq are d-q axis stator current, Ld and Lq are d-q axis inductance, ω is pulsation and φ_f: flux.

The torque is defined by [23]:

$$T_{em} = \frac{3}{2} p[(L_q - L_d) i_{ds} i_{qs} + i_{qs}\varphi_f] \quad (15)$$

Where *p* designates the number of poles pairs.

According to the principle of FOC, the electromagnetic torque depends only on the q-axis current component; we obtain then:

$$T_{em} = \frac{3}{2} p\, i_{qs}\, \varphi_f = K.i_{qs} \quad (16)$$

The dynamic of the PMSG rotor can be expressed as:

$$J\frac{d\omega}{dt} = T_m - T_e - B\omega \quad (17)$$

With J is the total inertia (kg m^2), B is viscous friction coefficient (kg m^2 /s), and Tm is the drive torque produced by wind turbine emulator.

According to equation (16), the PMSG speed can be controlled by the q-axis current component. As presented in figure 6, the reference speed from the MPPT device is used to generate the reference torque, and then the q-axis current component. The d-axis current component is set to zero.

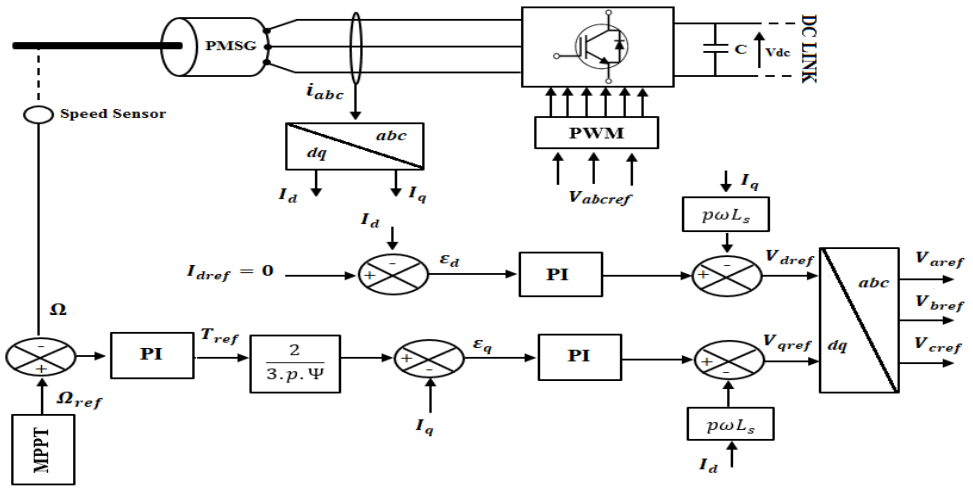

Fig.6. MPPT and FOC used to control the PMSG.

5. Control of grid-connected inverter

5.1. Voltage Oriented Control

The literature on the control of grid-connected inverter shows a variety of approaches. Such one is known as voltage-oriented control (VOC), as shown in figure 7. For the implementation of the VOC scheme, the grid voltages are measured to estimate the phase angle θg using phase-locked loop PLL. The variables are transformed from the abc stationary form to the dq synchronous form, and vice versa using the grid voltage angle θg [24-26].

Figure 7 shows a VOC system scheme.

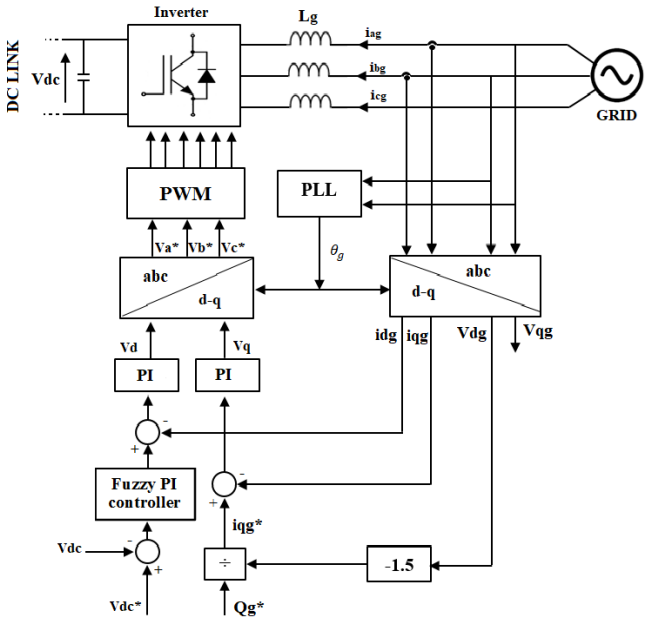

Fig.7. VOC system scheme.

The VOC system consists of three feedback control loops: one external feedback loop to regulate the DC-Link voltage, and two internal dq-axis currents loops. The active and reactive components of the grid currents iag, ibg, and icg are idg and iqg, respectively. These two components are controlled independently, which provide independent control of active and reactive power system.

The active and reactive powers are expressed as [27-28]:

$$\begin{cases} P_g = \frac{3}{2}\left(V_{dg}i_{dg} + V_{qg}i_{qg}\right) = \frac{3}{2}V_g i_{dg} \\ Q_g = \frac{3}{2}\left(V_{qg}i_{dg} - V_{dg}i_{qg}\right) = -\frac{3}{2}V_g i_{qg} \end{cases} \quad (18)$$

With Vqg = 0, since the VOC scheme aligns the grid voltage with the d-axis of the synchronous frame, i.e. ($V_{dg} = V_g$).

The transformation abc/dq or vice versa in our work preserves the amplitudes of voltages and currents.

According to equation (18), the setpoint of q-axis current i_{qg}^* is expressed as:

$$i_{qg}^* = -\frac{Q_g^*}{1.5V_g} \quad (19)$$

Where Q_g* represents the setpoint of reactive power.

The setpoint of the active power of the system is represented by the setpoint of dd-axis current i_{dg}* generated by the fuzzy adaptive PI controller for DC-Link voltage regulation. The DC-link voltage remains constant at a reference value Vdc*.

The equation that describes the DC-Link voltage system is as follows [29-35]:

$$C\frac{dV_{dc}}{dt} = \frac{3}{2}\frac{V_{dg}}{V_{dc}}i_{dg} - i_{ag} \quad (20)$$

With C represents the DC-Link capacity, Vdc represents the DC-link voltage.

5.2. Fuzzy adaptive PI controller

According to equation (20), The DC-Link system is nonlinear. Thus, the control of the external feedback loop of the DC-Link voltage could not perform accurately with linear control approaches. To overcome this issue, it is necessary to adopt a nonlinear approach, such as fuzzy logic control. It is presented in this work to substitute the Proportional-Integral PI controller.

In this work, a fuzzy adaptive PI controller is proposed, as presented in Figure 8. This type of control, called adaptive, allows exploiting the advantages presented by the PI controller and those of the fuzzy logic. The purpose of the adaptation law is to improve the control performance of complex and nonlinear systems.

The fuzzy adaptive PI controller changes its gain constant according to the error (e) between the setpoint value of the DC-link voltage and its measured value and the variation of error (Δe)[33]:

$$\begin{cases} e = V_{dc}^{*} - V_{dc} \\ \Delta e = e(t) - e(t-\Delta t) \end{cases} \quad (21)$$

The FLC generates the normalized signals ΔKp and ΔKi used to compute the gain of the PI controller:

$$\begin{cases} K_p = K_{p0} + G_p \Delta K_p(e, \Delta e) \\ K_i = K_{i0} + G_i \Delta K_i(e, \Delta e) \end{cases} \quad (22)$$

Where Kp represents the proportional gain, and Ki represents the integral gain. Kp0 and Ki0 are the two control parameters in the initial state; they are estimated using Ziegler and Nichols method. The values of the gains Gp and Gi are introduced since ΔKp1 and ΔKi1 are normalized quantities defined in the interval [-1, 1].

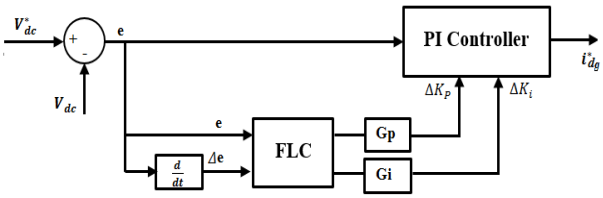

Fig. 8. Fuzzy adaptative PI for the control of the DC-link voltage.

The fuzzy system is used to modify in real-time the PI parameters according to the behavior of the process. Basically, Kp provides a fast-dynamic response while Ki eliminates the static error and ensures the stability of the system. When the error is large, Kp should be large and Ki small; when the error is small, Kp should be small and Ki large. Thus, specific rules in the fuzzy process can be built matrix to optimize the characteristics of the temporal response. The rule base chosen in this paper is reported in Table 3.

Table 3. Fuzzy logic rules**.**

ΔKp								
		e						
		HN	**N**	**lN**	**ZE**	**lP**	**P**	**HP**
Δe	**HN**	HN	HN	N	N	lN	ZE	ZE
	N	HN	HN	N	lN	lN	ZE	ZE
	lN	HN	P	lN	lN	ZE	lP	lP
	ZE	N	N	lN	ZE	lP	P	P
	lP	N	N	ZE	lP	lP	P	HP
	P	ZE	ZE	lP	lP	P	HP	HP
	HP	ZE	ZE	lP	P	P	HP	HP
ΔKi								
		e						
		HN	**N**	**lN**	**ZE**	**lP**	**P**	**HP**
Δe	**HN**	HP	HP	P	P	lP	ZE	ZE
	N	HP	HP	P	lP	lP	ZE	lN
	lN	P	P	P	lP	ZE	lN	lN
	ZE	P	P	lP	ZE	lN	N	N
	lP	lP	lP	ZE	lN	lN	N	N
	P	lP	ZE	lN	N	N	HN	HN
	HP	ZE	ZE	N	N	N	HN	HN

The abbreviations are defined as follows: HN is Huge Negative, N is Negative, lN is little Negative, ZE is Zero, HP is Huge Positive, P is positive, and lP is little Positive.

The logic for determining this matrix of rules is based on global or qualitative knowledge of how the system works. Indeed, it is completely normal to increase Kp and decrease Ki When the error is large; when the error is small, Kp should be small and Ki large. Table 3 summarizes all the rules of human know-how, it translates the rules expressed by the following common language:

- When the error *e* and its variation Δ*e* are large negatives (HN), ΔKp should be greatly decreased (HN) and ΔKi greatly increased (HP).
- When the error *e* and its variation Δ*e* are small negatives (lN), ΔKp should be greatly decreased (HN) and ΔKi greatly increased (HP).

6. Simulation and analysis

The complete WECS is simulated using the different models and control strategies presented in previous sections. The block diagram, integrating these various elements and forming the whole structure of a wind system, is given in figure 9.

The block of the induction motor model is controlled by a 2-level inverter using a FOC strategy to generate a mechanical torque depends on wind speed and different proprieties of the wind turbine for substituting the real wind turbine and to provide a testing environment for WECS control strategies in a controlled and safe environment. The PMSG is driven by the induction motor and controlled by a rectifier to maximize the maximizing captured power at different wind speeds. The inverter in

the grid side ensures the control and deliver the active and reactive power into the grid by keeping the DC-Link voltage constant.

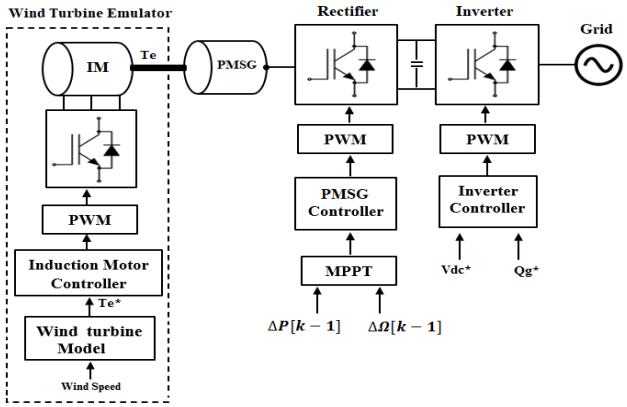

Fig.9. The entire structure of the wind system.

6.1. Emulation Results:

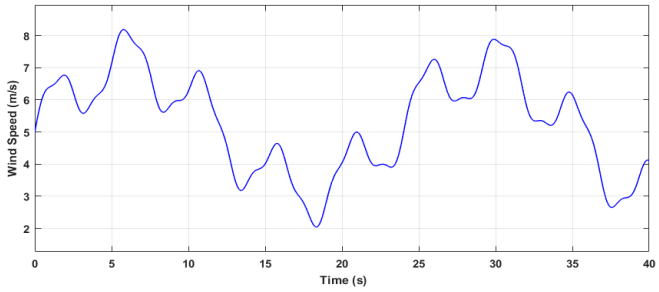

Fig. 10. Wind speed profile.

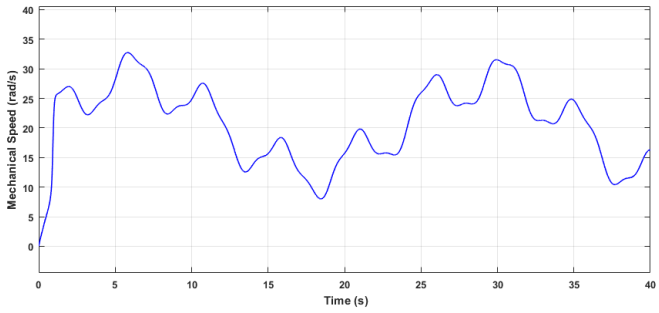

Fig.11. Speed of Induction Motor.

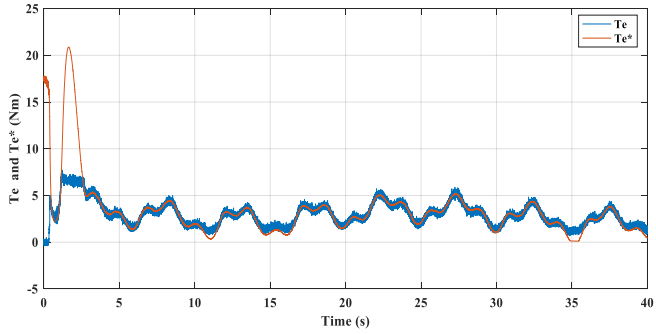

Fig. 12. The torque of Induction Motor.

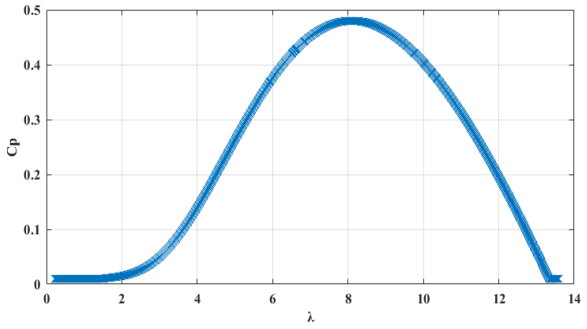

Fig. 13. Power coefficient Cp versus TSR λ.

Figures 11 and 12 represent the speed and the torque of the WTE, respectively. The variations of these correspond to the wind speed profile (figure 10) applied to the wind turbine model. The non-dimensional curve of power coefficient Cp versus TSR λ characterize the wind turbine Cp(λ) is represented in figure 13. For the optimum TSR (when λ = 8), the power coefficient is at maximum, and the wind turbine delivers the maximum of mechanical power.

The torque shown in Figure 12 corresponds to the reference torque from the wind turbine model, except for the moments at start where the reference torque is too high (the torque ordered has been limited for safety reasons).

The curve of the power coefficient C_p versus the TSR Tip Speed Ratio λ Cp(λ) characterizes the wind turbine, and it can be used to achieve MPPT (Maximum Power Point Tracking) for an Optimal TSR (λ = 8) the power coefficient C_p is maximum.

6.2. MPPT Results:

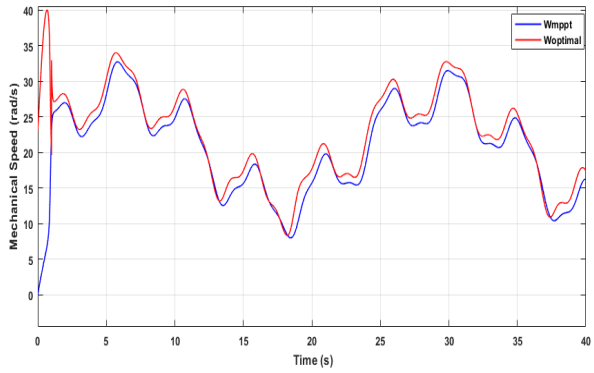

Fig. 14. Mechanical speed and optimal speed of PMSG.

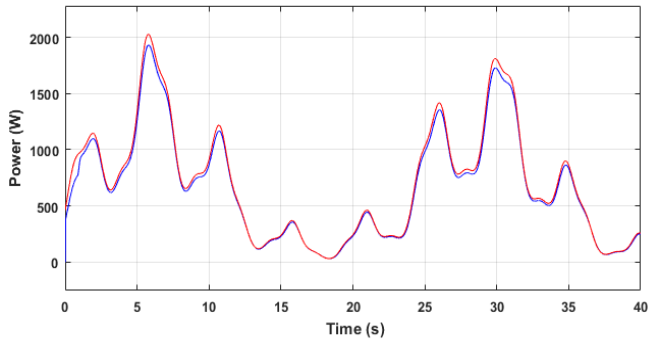

Fig. 15. Mechanical power and optimal power of PMSG.

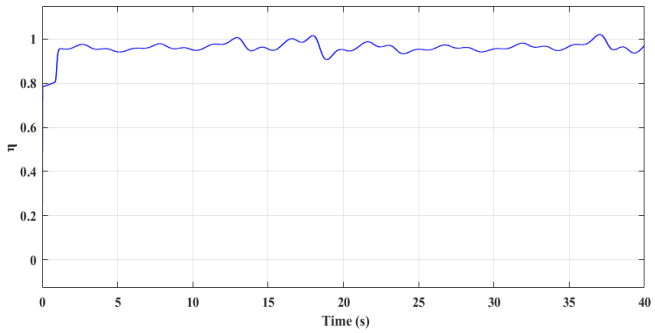

Fig. 16. The efficiency obtained thanks to fuzzy MPPT.

Figure 14 shows the mechanical speed of PMSG optimized by the fuzzy MPPT compared to the curve of the optimal rotation speed calculated according to equation (23):

$$\Omega_{opt} = \frac{\lambda_{opt}\, v}{R} \tag{23}$$

The mechanical speed of PMSG determines the operating point relative to the maximum powerpoint. The difference between the MPPT speed and the optimal speed is then reflected in a power loss shown in figure 15. The optimal power curve calculated using expression (24):

$$P_{opt} = \frac{1}{2}.C_p^{opt}.\rho.S.v^3 \tag{24}$$

Figure 16 represents the efficiency of the system calculated according to equation (25):

As can be depicted in figure 16 the algorithm is reliable with an efficiency of 88%.

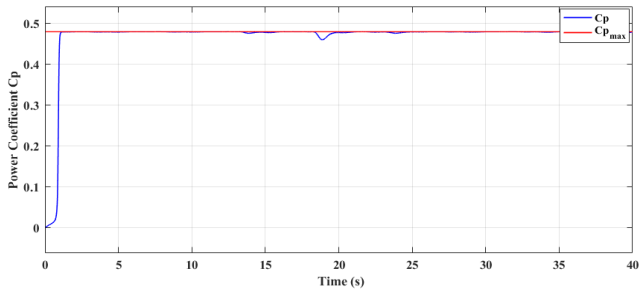

Fig. 17. Power coefficient of the wind turbine.

When the wind energy conversion system operates under MPPT control, the power coefficient Cp of the wind turbine is maintained to its maximum value (Cpmax=0.48), as it can be depicted in figure 17.

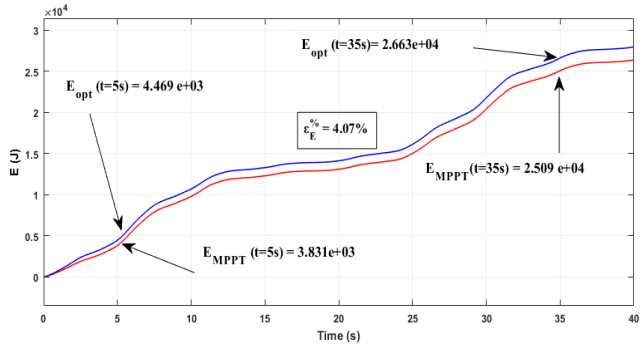

Fig. 18. Optimal wind energy and optimized wind energy by the proposed MPPT device.

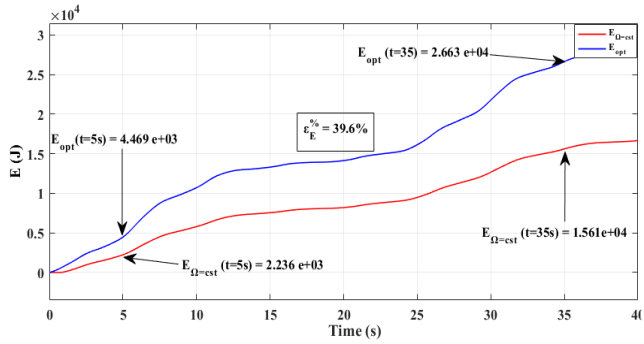

Fig. 19. Optimal wind energy and wind energy without MPPT device.

The difference between the optimal energy and that from the MPPT device gives a quantified overview of the

$$\eta = \frac{P_{MPPT}}{P_{opt}} \tag{25}$$

quality of the energy extraction over a given period and a representation of the energy "captured" by the system, which is a relevant criterion of appreciation of energy efficiency.

The difference calculated using equation (28):

$$E = \int_{t_1}^{t_2} P(V)\, dt \qquad (26)$$

$$\Delta E = E(t = t_2) - E(t = t_1) \qquad (27)$$

$$\varepsilon_E^{\%} = \frac{\Delta E_{opt} - \Delta E_{MPPT}}{\Delta E_{opt}} \qquad (28)$$

The total energy optimized by MPPT device and the maximum energy which can be extracted from a given wind profile during the test time (figure 18) delivers a difference of 4.07%. However, this energy difference is worth 39.6% (figure 19) for an equivalent system, but operating at a constant speed, i.e., without MPPT device. Which allows an energy gain offered by the MPPT device of 35.5%.

6.3. Grid-connected system results

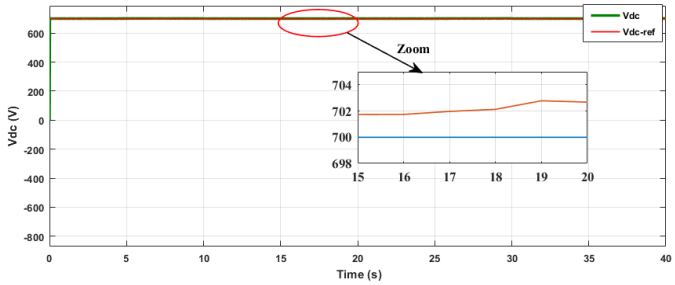

Fig. 20. DC-Link Voltage.

Figure 20 presents the measured DC-Link voltage controlled by a Fuzzy adaptive PI controller, where it reveals nearly no voltage fluctuation, with a steady-state error equal 2V, which represents 0.29% of the reference voltage value 700V.

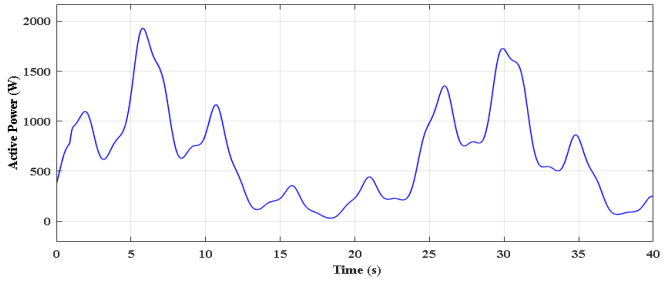

Fig. 21. Active Power.

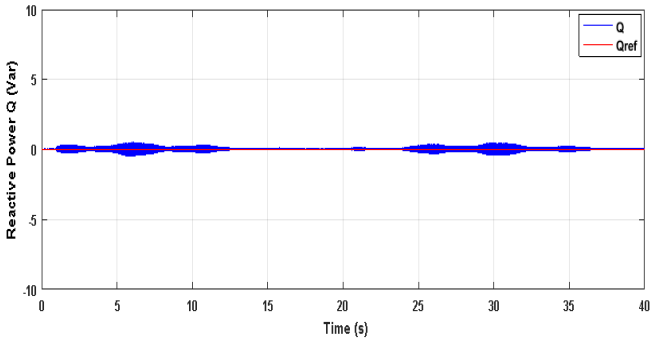

Fig. 22. Reactive Power.

The active and reactive powers of the grid are presented in figure 21 and figure 22, respectively. As mentioned above, the active and reactive powers are controlled independently. The active power is stabilized, and the reactive power equals zero, which corresponds to operation with a unity power factor.

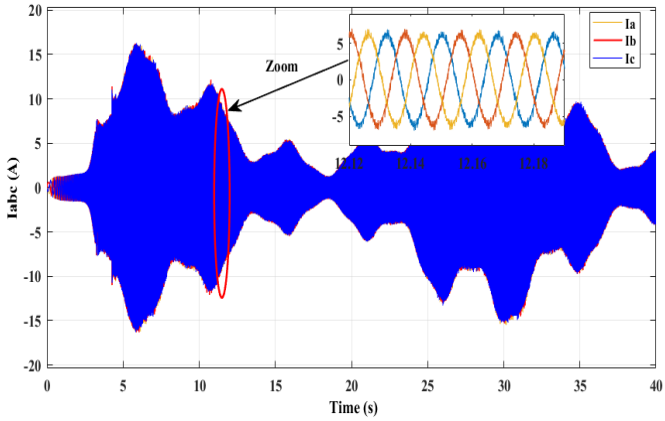

Fig. 23. Currents injected into the grid.

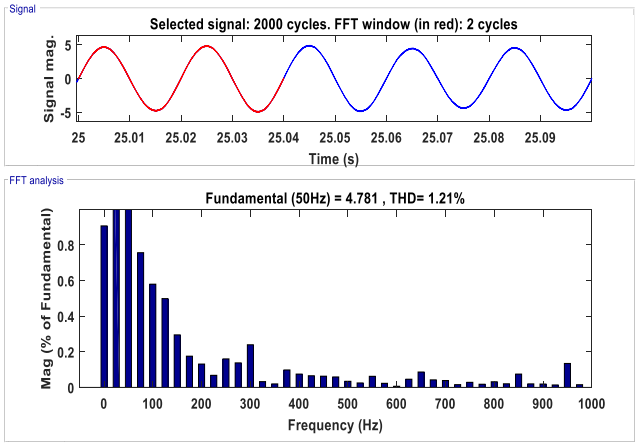

Fig. 24. Signal and Fast Fourier Transform FFT analysis of the current signal.

The currents injected to the electrical grid results are shown in Figure 23. To investigate the quality of the power injected to the grid, the fundamental and harmonic

components in the current injected to the grid signal are extracted using the Powergui FFT Analysis Tool in MATLAB. As it can be illustrated in figure 24, the fundamental current supplied to the grid equals 4.78A, and the total harmonic distortion THD is 1.21 %.

7. Conclusion

This work deals with a nonlinear control approach of the variable-speed WECS consists of the PMSG connected to the electrical grid through back-to-back converters.

The fuzzy logic approach is used to implement the (MPPT) and DC bus voltage regulation. The nonlinear control strategy based on the fuzzy logic suggested in this work can overcome the non-linearity of the DC-Link voltage system and ensure a dynamic and reliable control of the PMSG with desired maximum power without the knowledge of the turbine characteristics curve Cp(λ).

An experimental evaluation of the simulation results will be treated as the future scope of this work.

Appendix

Table 4. Parameters of the proposed WECS

Parameters of the wind turbine model	
Parameter	**Value**
ρ **the air densityy**	1.225 kg/m3
R the radius of the blades	2.5 m
Parameters of Induction motor	
Parameter	**Value**
Pr rated power	3Kw
ωm rated mechanical speed	1430 rpm
R stator resistance	2.3 Ω
Ls stator d-axis inductance	163mH
Parameters of the PMSG	
Parameter	**Value**
Stator resistance Rs(Ω)	1.137
Stator d-axis inductance Ld (mH)	2.7
Stator q-axis inductance Lq (mH)	2.7
Flux ϕ **(Wb)**	0.15
P poles pairs number	17
Parameters of the grid side	
Parameter	**Value**
V_{dc}^{*} **DC-Link Voltage reference(V)**	700V
C DC-Link capacitor (mF)	50
R Filter resistance (Ω)	0.5
L Filter inductance (mH)	25

References

[1] D.A CIUPAGEANU, G. LAZAROIU, L. BARELLI. Wind Energy Integration: Variability Analysis and Power System Impact Assessment. Energy, Volume 185, 15 October 2019, Pages 1183-1196.

[2] B. Wu, Y. Lang, N. Zargari, S. Kouro, Power Conversion and Control of Wind Energy Systems, New Jersey: IEEE Press, 2011.

[3] S. Bououden, M. Chadli, S.Filali, A.El Hajjaji. Fuzzy model-based multivariable predictive control of a variable speed wind turbine: LMI approach. Renewable Energy, Vol 37, Issue 1, January 2012, Pages 434-439.

[4] W. Meng; Q. Yang; Y. Ying; Y. Sun; Z. Yang; Sun. Adaptive Power Capture Control of Variable-Speed Wind Energy Conversion Systems With Guaranteed Transient and Steady-State Performance, IEEE Transactions on Energy Conversion, Volume: 28, Issue: 3, Sept. 2013.

[5] K. Kim; T. L. Van; D. Lee; S. Song. Maximum Output Power Tracking Control in Variable-Speed Wind Turbine Systems Considering Rotor Inertial Power. IEEE Transactions on Industrial Electronics, Volume: 60, Issue: 8, Aug. 2013.

[6] T. Nguyen; D. Lee. Advanced Fault Ride-Through Technique for PMSG Wind Turbine Systems Using Line-Side Converter as STATCOM. IEEE Transactions on Industrial Electronics, Volume: 60, Issue: 7, July 2013.

[7] M. Wenchao, Y. Qinmin, Y. You, S. Yong, S. Youxian. Adaptive Power Acquisition Control of Variable-speed Wind Energy Conversion Systems under Inaccurate Wind Speed Measurement, IEEE-American Control Conference (ACC); June 2013, p. 4271-6.

[8] Z. Zhenbin, H. Christoph, W. Fengxiang, C. Zhe, K. Ralph. Encorderless model predictive control of back-to-back converter direct-drive permanent-magnet synchronous generator wind turbine systems. 15th IEEE-European conference on power electronics and applications (EPE); September 2013, p,1-10.

[9] X. Changliang, W. Zhiqiang, S. Tingna, S. Zhanfeng. A novel cascaded boost chopper for the wind energy conversion system based on the permanent magnet synchronous generator. IEEE Trans Energy Conversion 2013, 28 (3):512-22.

[10] H. Matayoshi, A. M. Howlader, M., Datta, T. Senjyu. Control strategy of PMSG based wind energy conversion system under strong wind conditions. Energy for Sustainable Development, Vol: 45, August 2018, Pages 211-2018.

[11] M. H. Qais, H. M. Hasanien, S. Alghuwainem. Augmented grey wolf optimizer for grid-connected PMSG-based wind energy conversion systems. Applied Soft Computing, Vol:69, August 2018, Pages 504-515.

[12] Qu keqing, Niu Qingquan, Li Jie. A MPPT vector control method for wind power PMSG system. In: Proceeding of the 7th interational power electronics and motion control conference (IPEMC), Vol.2; June 2012, p. 1264-7.

[13] Shuhi Li, Haskew TA, Swatloski RP, Gathings W. Optimal and direct-current vector control of direct-driven PMSG wind turbines. IEEE Trans Power Electron 2012; 27(5): 2325-37.

[14] Abdullah MA, Yatim AHM, Tan Chee Wei. A study of maximum power point tracking algorithms for wind energy system. Proceeding of clean energy and technology (CET), IEEE first conference on; 2011, p. 321-6

[15] J. Pramod. Wind energy engineering. McGraw-HillISBN:978-0-07-171477-8, MHID:0-07-171477-4, P:1024,2011.

[16] K. Trinadha, A. Kumar, K. S. Sandhu. Study of Wind Turbine based SEIG under Balanced/Unbalanced Loads and Excitation, International Journal of Electrical and Computer Engineering (IJECE), Vol.2, No.3, June 2012, pp. 353 370.

[17] S. Heier. Grid Integration of Wind Energy Conversion Systems. John Wiley & Sons Ltd, 1998.

[18] A.S. Bazanella, R. Reginatto. Robust tuning of the speed loop in indirect field oriented control of induction motors. Automatica, Vol 37, p:1811-1818,2001.

[19] A. M. Eltamaly; H. M. Farh. Maximum power extraction from the wind energy system based on fuzzy logic control. Electric Power Systems Research, Volume 97, April 2013, Pages 144-150.

[20] Hong Chih-Ming, Chen Chiung-Hsing, Chia-Sheng Tu. Maximum power point tracking-based control algorithm for the PMSG wind generation system without mechanical sensors. Energy Convers Manage 2013; 6:58–67.

[21] E. G. Shehata. A comparative study of current control schemes for a direct-driven PMSG wind energy generation system. Electric Power Systems Research, Volume 143, February 2017, Pages 197-205.

[22] Shenquqn Li, Kezhao zhang, Juan Li, Chao liu, ‘ On the rejection of internal and external disturbances in a wind energy conversion system with direct-driven PMSG’, ISA Transactions, 2016, 61 , pp. 95-103.

[23] L. S. Barros, C. M. V. Barros. An internal model control for enhanced grid-connection of direct-driven PMSG-based wind generators. Electric Power Systems Research, Volume 151, October 2017, Pages 440-450.

[24] N. Phankong, S. Manmai, K. Bhumkittipich, P. Nakawiwat. Modeling of Grid-connected with Permanent Magnet Synchronous Generator (PMSG) Using Voltage Vector Control. Energy Procedia, Volume 34, 2013, Pages 262-272.

[25] M., Zarif, M. Monfared. Step-by-step design and tuning of VOC control loops for grid-connected rectifiers. International Journal of Electrical Power & Energy Systems, Vol 64, January 2015, Pages 708-713.

[26] Ahmed G. Abo-Khalil. Grid Connection Control of DFIG in Variable Speed Wind Turbines under Turbulent Conditions. International Journal of Renewable Energy Research, Vol.9, No.3, September 2019.

[27] S. Zhang; K. Tseng; D. Vilathgamuwa; T. Nguyen; Xiao-Yu Wang. Design of a Robust Grid Interface System for PMSG-Based Wind Turbine Generators. IEEE Transactions on Industrial Electronics. Volume: 58, Issue: 1, Jan. 2011.

[28] Bhavna Jain, Shailendra Jain, R. K. Nema. Control strategies of grid interfaced wind energy conversion system: An overview. Renewable and Sustainable Energy Reviews, Vol 47, July 2015, Pages 983-996.

[29] E. Aydin, A. Polat, L. T. Ergene. Vector Control of DFIG in Wind Power Applications. 5th International Conference on Renewable Energy Research and Applications ICRERA2016, 20-23 November 2016, Birmingham, UK.

[30] J. Zhang, M. Cheng. DC Link Voltage Control Strategy of Grid-connected Wind Power Generation System. 2nd IEEE ISPElDGS, Hefei, China, 2010, pp. 970-975.

[31] P. Tourou, J. Chhor, K. Gunther and C. Sourkounis. Energy Storage Integration in DFIG-based Wind Energy Conversion Systems for Improved Fault Ride-Through Capability. 6th International Conference on Renewable Energy Research and Applications ICRERA2016, 5-8 November 2017, San Diego, USA.

[32] A. Hassoune, M. Khafallah, A. Mesbahi, T. Bouragba, Power Management Strategies of Electric Vehicle Charging Station Based Grid Tied PV-Battery System, International Journal of Renewable Energy Research, Vol.8, No.2, June, 2018.

[33] C. Viveiros, R. Melício, J.M. Igreja and V.M.F. Mendes, Wind Energy Conversion System Control using Distinct Controllers for Different Operating Regions, 4th International Conference on Renewable Energy Research and Applications ICRERA2016, 22-25 November 2017, Palermo, Italy.

[34] E. Hamatwi, IE Davidson, M N Gitau, Control of multi-level Voltage Source Converters Integrating a Wind Turbine System into the Grid, 5th International Conference on Renewable Energy Research and Applications ICRERA2016, 20-23 November 2016, Birmingham, UK.

[35] P. Stumpf, I. Nagy, I. Vajk, Novel Approach of Microgrid Control, 3th International Conference on Renewable Energy Research and Applications ICRERA2016, 5-8 October 2014, Milwakuee, USA.